KamLAND's Precision Measurement of Neutrino Oscillation Parameters

M. Patrick Decowski for the KamLAND Collaboration

Department of Physics, University of California, Berkeley, CA 94720, USA

E-mail: decowski@berkeley.edu

Abstract. The KamLAND experiment uses reactor antineutrinos to study the solar neutrino oscillation parameters. KamLAND recently updated the reactor neutrino measurement, with an almost fourfold increase of the exposure, an improved analysis technique and better understanding of the backgrounds and systematic uncertainties. Extending the analysis down to the inverse beta decay energy threshold gives a best-fit at $\Delta m^2_{21} = 7.58^{+0.14}_{-0.13}(\mathrm{stat})^{+0.15}_{-0.15}(\mathrm{syst}) \times 10^{-5}\,\mathrm{eV}^2$ and $\tan^2\theta_{12} = 0.56^{+0.10}_{-0.07}(\mathrm{stat})^{+0.10}_{-0.06}(\mathrm{syst})$. Local $\Delta\chi^2$-minima at higher and lower Δm^2_{21} are now disfavored at $>4\sigma$. When combined with solar neutrino data, we obtain $\Delta m^2_{21} = 7.59^{+0.21}_{-0.21} \times 10^{-5}\,\mathrm{eV}^2$ and $\tan^2\theta_{12} = 0.47^{+0.06}_{-0.05}$. KamLAND is presently purifying the detector to measure solar ^{7}Be neutrinos in the near future.

1. Introduction

Nuclear reactors emit electron antineutrinos ($\overline{\nu}_e$) isotropically during the decay of neutron-rich radioactive products of the fission process. The Kamioka Liquid scintillator Anti-Neutrino Detector (KamLAND) investigates neutrino oscillation parameters by observing electron antineutrinos emitted from distant nuclear reactors.

The $\overline{\nu}_e$ spectrum emitted by commercial reactors can be calculated with $\sim$2% uncertainty from $\overline{\nu}_e$ spectra and the reactor fission rates for ^{235}U, ^{238}U, ^{239}Pu and ^{241}Pu provided by the power companies operating the reactors. The average reactor $\overline{\nu}_e$ energy is $\sim$4 MeV. Since the $\overline{\nu}_e$-survival probability function depends on E_ν explicitly, any oscillatory behavior will manifest itself in a distortion of the measured neutrino energy spectrum.

KamLAND, a 1 kton liquid scintillator detector, is situated in the old Kamiokande cavity in a horizontal shaft mine in the Japanese Alps at a depth of $\sim$2700 m water equivalent. The site is surrounded by 55 Japanese commercial power reactors, at a flux weighted average distance of 180 km. This baseline makes KamLAND sensitive to the neutrino mass-splitting associated with the solar neutrino problem and in particular to the large mixing angle (LMA) solution. A description of KamLAND can be found in Ref. [1].

Electron antineutrinos are detected via inverse β-decay, $\overline{\nu}_e + p \rightarrow e^+ + n$, which has a 1.8 MeV $\overline{\nu}_e$ energy threshold. The prompt scintillation light from the e^+ gives an estimate of the incident $\overline{\nu}_e$ energy, $E_{\overline{\nu}_e} = E_\mathrm{p} + \overline{E}_n + 0.8\,\mathrm{MeV}$, where E_p is the prompt event energy including the positron kinetic energy and the annihilation energy, and $\overline{E}_n$ is the average neutron recoil energy, which is typically a few tens of keV. The neutron captures on hydrogen $207.5 \pm 2.8\,\mu s$ later, giving off a characteristic 2.2 MeV γ ray. This delayed coincidence is a powerful tool for reducing background.

2. Analysis Cuts and Systematic Uncertainties

The results presented here are based on data collected from March 9, 2002 to May 12, 2007; together with a 6-m-radius fiducial volume, the total exposure is 2.44×10^{32} proton-yr (2881 ton-yr). We recently commissioned an "off-axis" calibration system capable of positioning radioactive sources away from the central vertical axis of the detector. The system allowed us to reduce the fiducial volume uncertainty from 4.7% [2] to 1.6% for R <5.5 m and 1.8% for R <6 m. This, combined with other systematic uncertainties such as those arising from the $\overline{\nu}_e$-spectra (2.4%), reactor power (2.1%), the energy threshold (1.5%), fuel composition (1.0%) and various smaller contributions gives an expected event rate uncertainty of 4.1%. This uncertainty primarily affects the determination of θ_{12}. The uncertainty on Δm^2_{21} is mostly determined by the energy scale uncertainty (1.9%); the total Δm^2_{21} systematic uncertainty is estimated to be 2.0%.

The present analysis is over the full reactor spectrum and we require $0.9\,\mathrm{MeV} < E_\mathrm{p} < 8.5\,\mathrm{MeV}$. The neutron predominantly captures on protons and the delayed energy requirement for this reaction is $1.8\,\mathrm{MeV} < E_\mathrm{d} < 2.6\,\mathrm{MeV}$. However, occasionally the neutron captures on ^{12}C and we also allow $4.0\,\mathrm{MeV} < E_\mathrm{d} < 5.8\,\mathrm{MeV}$. The time difference ($\Delta T$) and distance ($\Delta R$) between the prompt positron and the delayed neutron are required to be $0.5\,\mu\mathrm{s} < \Delta T < 1000\,\mu\mathrm{s}$ and $\Delta R < 2\,\mathrm{m}$, respectively. The size of the effective fiducial volume with good signal-to-background is limited because of the rapidly increasing accidental coincidence rate from backgrounds near the balloon surface ($R = 6.5\,\mathrm{m}$). For this analysis we introduced a more effective constraint on event characteristics to better suppress accidental backgrounds while maintaining high efficiency, allowing a larger fiducial volume. The prompt and delayed radial distance from detector center (R_p, R_d) must be less than 6 m. To discriminate signal from background, we construct a multi-dimensional probability density function (PDF) for accidental coincidence events, f_{acc}, by pairing events in a delayed-coincidence window between 10 ms and 20 s. Using GEANT4 simulations, we construct a PDF for the $\overline{\nu}_e$ signal, $f_{\overline{\nu}_e}$, generating prompt and delayed events using the measured neutron capture time and detector energy resolution. For the E_p distribution in $f_{\overline{\nu}_e}$, we choose an oscillation-free reactor spectrum including a contribution from geoneutrinos estimated from a geological reference model [3]. A discriminator value, $L = \frac{f_{\overline{\nu}_e}}{f_{\overline{\nu}_e}+f_{acc}}$, is calculated for each candidate pair that passes the earlier cuts. To discriminate $\overline{\nu}_e$-candidates from accidental-background we establish a selection value $L_i^{cut}(E_\mathrm{p})$ in prompt energy intervals of 0.1 MeV optimized for maximal signal sensitivity ($L > L_i^{cut}(E_\mathrm{p})$ for signal-like events). $L_i^{cut}(E_\mathrm{p})$ is the value of L at which the figure-of-merit, $\frac{S_i}{\sqrt{S_i+B_i}}$ is maximal, where S_i and B_i are the number of signal and accidental-background events in the ith energy bin calculated from $f_{\overline{\nu}_e}$ and f_{acc}, respectively.

The selection efficiency $\epsilon(E_\mathrm{p})$ is estimated from the fraction of selected coincidence events relative to the total generated in $\mathrm{R} < 6\,\mathrm{m}$ in the simulation, see Fig. 1(top). The increasing accidental rate at low energies results in a lower efficiency. Above the ^{208}Tl Compton shoulder at 2.6 MeV, ϵ reaches 93% reflecting the efficiency of spatial and temporal cuts (R_p, R_d, ΔR, ΔT) alone.

3. Backgrounds

The dominant background is caused by α-induced neutron background from $^{13}\mathrm{C}(\alpha,\mathrm{n})^{16}\mathrm{O}$ reactions. The prime α particle source is the decay of ^{210}Po, a daughter of the ^{222}Rn decay-chain introduced into the scintillating fluid during assembly. We estimate there were $(5.56 \pm 0.22) \times 10^9$ ^{210}Po α particle decays in the full data-set, by observing the quenched scintillation signal from the 5.3 MeV α particle. While the ^{13}C abundance is only 1.1% of the carbon in the LS, the reaction rate is significant resulting in neutrons with energies up to 7.3 MeV. These neutrons scatter elastically off protons and since the observable proton ionization loss is quenched, most of the observed scintillation energy spectrum is below 2.7 MeV. In addition, the

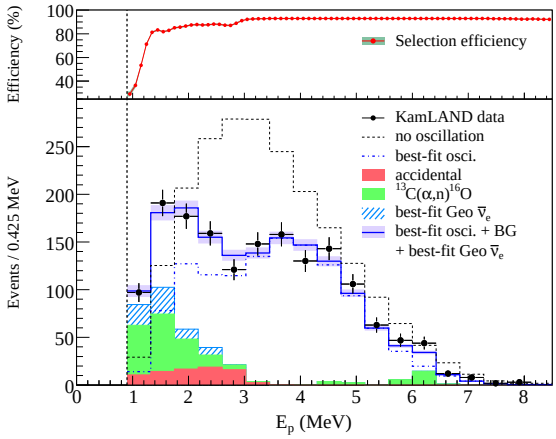

Figure 1. Prompt event energy spectrum of $\bar{\nu}_e$ candidate events. All histograms corresponding to reactor spectra and expected backgrounds incorporate the energy-dependent selection efficiency (top panel). The shaded background and geoneutrino histograms are cumulative. The data show the statistical uncertainties, the band on the blue histogram indicates the event rate systematic uncertainty.

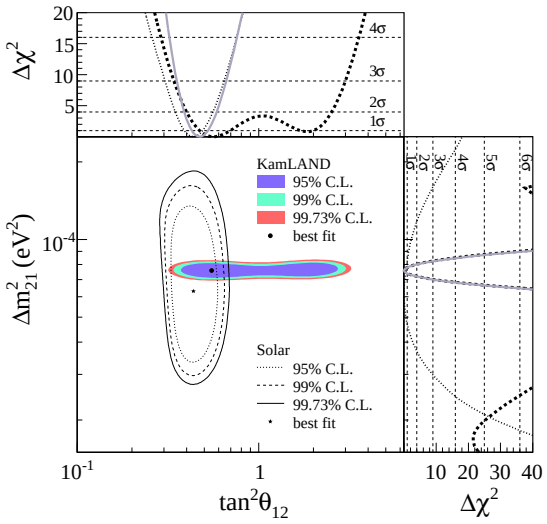

Figure 2. Allowed region for neutrino oscillation parameters from KamLAND and solar neutrino experiments. The side-panels show the $\Delta\chi^2$-profiles for KamLAND (dashed) and solar experiments (dotted) individually, as well as the combination of the two (solid).

1st (6.05 MeV, e^+e^-) and 2nd (6.13 MeV γ) excited states of ^{16}O and ^{12}C(n,n')^{12}C* (4.4 MeV γ) produce coincidences with the scattered neutron. The exact cross sections of the ^{16}O excited states are not well known. A ^{210}Po^{13}C source was employed to study the ^{13}C(α,n)^{16}O reaction and to calibrate our Monte Carlo code, including the source encapsulation, that uses ^{13}C(α,n)^{16}O reaction cross sections from Ref. [4, 5]. We convert the energies of the neutrons to visible energies using proton quenching factors obtained from a measurement at an intense neutron source facility. We find that the cross sections for the excited ^{16}O states from Ref. [4] agree with the ^{210}Po^{13}C data after scaling the 1st excited state by 0.6; the 2nd excited state requires no scaling. For the ground-state we use the cross section from Ref. [5] after subtracting the scaled excited states while accounting for the energy-dependent neutron detection efficiency [6] and scaling the resulting spectrum by 1.05. Including the ^{210}Po decay-rate, we assign an uncertainty of 11% for the ground-state and 20% for the excited states. The total ^{13}C(α,n)^{16}O background in the full data-set is 182±21.7 events.

The accidental coincidence background is measured with a 10 ms to 20 s delayed-coincidence window, the expected background is 80.5±0.1 events. Spallation-produced neutrons ($<$ 9.0 background events) are suppressed by incorporating a 2 ms full-volume veto after a detected muon in the analysis. For the cosmogenic beta delayed-neutron emitters ^{9}Li and ^{8}He, we apply a 2 s veto within a 3-m-radius cylinder around well-identified muon tracks passing the detector or a 2 s veto of the full detector for muons that either deposit a large amount of energy or that cannot be tracked. We estimate that 13.6±1.0 ^{9}Li/^{8}He events remain.

Finally, for the neutrino oscillation measurement there is also a background from antineutrinos produced in the decay chains of ^{232}Th and ^{238}U in the Earth's interior [3]. These so-called geoneutrinos are limited to prompt energies below 2.6 MeV. Our analysis takes geoneutrinos into account and simultaneously fits for geoneutrinos and neutrino oscillation

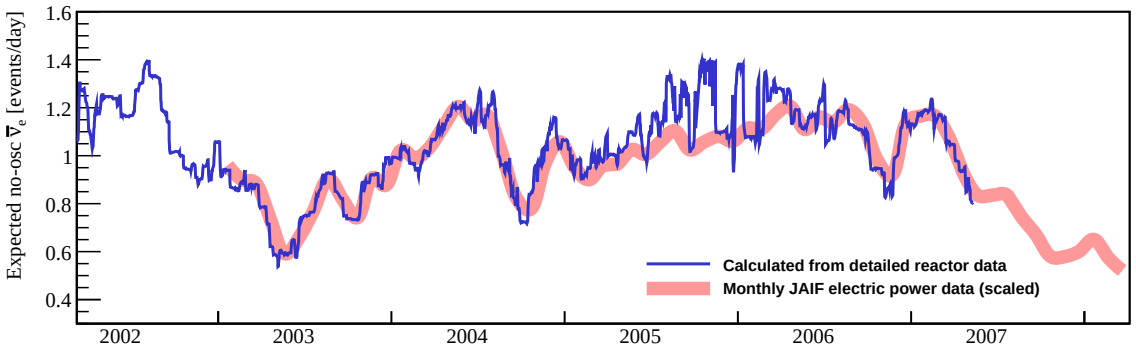

Figure 3. Estimated time variation of the reactor $\overline{\nu}_e$ flux at KamLAND assuming no antineutrino oscillation. The black line shows the flux variation calculated from detailed reactor operational records, the thicker pink line indicates the time variation calculated from the JAIF monthly electrical power report and scaled to match the calculated $\overline{\nu}_e$ variation in the period 2003–2004. The large differences between the two curves in late 2005 is due to the fact that one nearby reactor was being commissioned, but not yet part of the electrical grid. The flux was particularly low in late 2007/early 2008, improving the signal-to-background ratio for geoneutrino detection.

parameters, see [7] of these proceedings.

4. Neutrino Oscillation Analysis

Figure 1 shows the prompt energy spectrum of identified electron antineutrino events and the expected background. The unbinned data are assessed with a maximum likelihood fit to two-flavor neutrino oscillation simultaneously fitting the geoneutrino contribution. The method incorporates the absolute time of the event to account for time variations in the reactor flux (the so-called "rate-shape-time" analysis) and takes into account Earth-matter effects. The background includes contributions from ^{9}Li, accidental, ^{13}C(α,n)^{16}O and geoneutrino spectra. The amplitude of the geoneutrino contribution from uranium and thorium is not constrained because of large geological uncertainties. The fitted spectrum for the rate-shape-time analysis is shown in Fig. 1; the joint confidence intervals give $\Delta m^2_{21} = 7.58^{+0.14}_{-0.13}(\mathrm{stat})^{+0.15}_{-0.15}(\mathrm{syst}) \times 10^{-5}\,\mathrm{eV}^2$ and $\tan^2\theta_{12} = 0.56^{+0.10}_{-0.07}(\mathrm{stat})^{+0.10}_{-0.06}(\mathrm{syst})$ for $\tan^2\theta_{12}<1$. The present data excludes a scaled reactor spectrum with no distortion from neutrino oscillation at 5σ.

The allowed parameter contours for the rate-shape-time analysis, including $\Delta\chi^2$-profiles, are shown in Fig. 2. With the current KamLAND data, the so-called LMA I region remains, the other parameter regions that were previously allowed by KamLAND are disfavored at more than $4\,\sigma$. The parameter space can be further constrained by incorporating the results from solar experiments [8, 9] in a two-neutrino analysis with KamLAND. Under the assumption of CPT invariance, the combined analysis gives $\Delta m^2_{21} = 7.59^{+0.21}_{-0.21} \times 10^{-5}\,\mathrm{eV}^2$ and $\tan^2\theta_{12} = 0.47^{+0.06}_{-0.05}$.

5. Reactor Power Variation and Limits on a "Geo-Reactor"

The power produced by nuclear reactors varies over time, due to refueling cycles and periodic inspections. Fig. 3 shows the estimated time variation of the $\overline{\nu}_e$ flux at KamLAND under the assumption of no $\overline{\nu}_e$ oscillation. The figure shows the flux as calculated from the detailed reactor

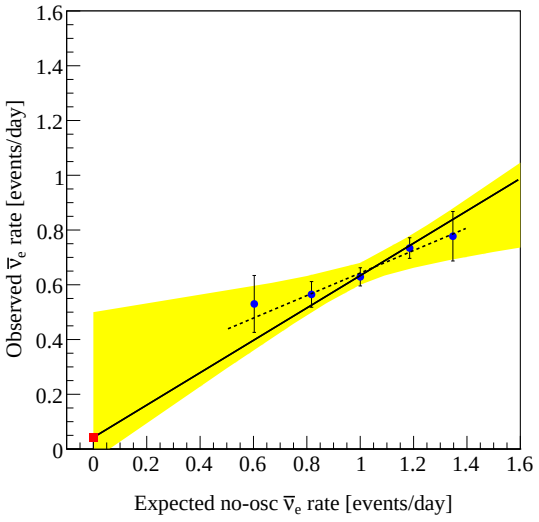

Figure 4. Observed $\overline{\nu}_e$ event rate versus no-oscillation reactor $\overline{\nu}_e$ flux. Data points correspond to intervals of approximately equal $\overline{\nu}_e$ flux. The dashed line is a fit, the 90% C.L. is shown in yellow. The solid line is a fit constrained to the expected background (red point). The low reactor neutrino flux from mid-2007 to 2008 (see Fig. 3), will allow KamLAND to put more stringent constraints on this correlation.

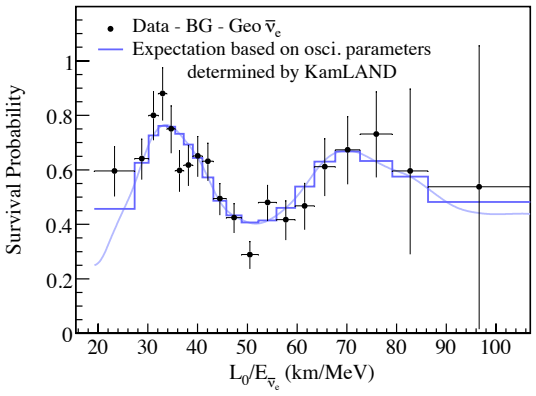

Figure 5. Ratio of the background and geoneutrino subtracted $\overline{\nu}_e$ spectrum to the expectation for no-oscillation as a function of L_0/E. L_0 is the effective baseline taken as a flux-weighted average ($L_0 = 180$ km); the energy bins are equal probability bins of the best-fit including all backgrounds (see Fig. 1). The histogram and curve show the expectation accounting for the distances to the individual reactors, time-dependent flux variations and efficiencies. The error bars are statistical and do not include correlated systematic uncertainties in the energy scale.

operational records of all 55 Japanese reactors and a similar calculation from monthly power production data published by JAIF[10], scaled to match the detailed calculation in the period 2003 to 2004. The disagreement between the two calculations in late 2005 is due to the fact that one powerful nearby reactor, Chika-2, was being commissioned while not yet producing electricity for the grid. The powerful Kashiwazaki complex (24 GW_{th} total thermal power at 160 km from KamLAND) on the other hand has been offline since an earthquake occurred on July 17, 2007, providing an opportunity for measurements with low incident $\overline{\nu}_e$ flux.

Figure 4 shows the signal counts plotted in bins of approximately equal $\overline{\nu}_e$ flux corresponding to total reactor power. For the Δm^2_{21} and $\tan^2\theta_{12}$ determined above and the known distributions of reactor power level and distance, the expected oscillated $\overline{\nu}_e$ rate is well approximated by a straight line. The slope can be interpreted as the $\overline{\nu}_e$ rate suppression factor and the intercept as the reactor-independent constant background rate. The intercept is consistent with known backgrounds, and limits a possible geo-reactor at the center of the Earth to <6.2 TW at 90% C.L.

The ratio of the background-subtracted $\overline{\nu}_e$ candidate events, including the subtraction of geoneutrinos, to no-oscillation expectation is plotted in Fig. 5 as a function of L_0/E. The spectrum indicates almost two cycles of the periodic feature expected from neutrino oscillation.

6. Detecting Solar Neutrinos

The KamLAND experiment is presently purifying the liquid scintillator for the low-background phase of the experiment. The aim of this phase is to measure solar ^{7}Be and possibly CNO/*pep* neutrinos through elastic scattering. The challenge is to reduce the background sufficiently; the background contributions of ^{40}K, ^{85}Kr and ^{210}Pb have to be reduced by 10^2, 10^6 and 10^5, respectively. The first purification engineering run (May–August 2007) showed a modest reduction in backgrounds and several improvements were subsequently implemented. A new purification campaign started in May 2008 and will run until December 2008.

7. Conclusions

The KamLAND results confirm neutrino oscillation, providing the most precise value of Δm^2_{21} to date and improving the precision of $\tan^2\theta_{12}$ in combination with solar neutrino data. Only one allowed region in the neutrino oscillation parameter space remains in the solar sector.

References

[1] S. Abe *et al.* [KamLAND Collaboration], Phys. Rev. Lett. **100**, 221803 (2008) [arXiv:0801.4589 [hep-ex]].
[2] T. Araki *et al.* [KamLAND Collaboration], Phys. Rev. Lett. **94**, 081801 (2005) [arXiv:hep-ex/0406035].
[3] S. Enomoto, E. Ohtani, K. Inoue and A. Suzuki, Earth Planet. Sci. Lett. **258**, 147 (2007).
[4] JENDL, the Japanese Evaluated Nuclear Data Library available at http://wwwndc.tokai-sc.jaea.go.jp/jendl/jendl.html (2005).
[5] S. Harissopulos, H. W. Becker, J. W. Hammer, A. Lagoyannis, C. Rolfs and F. Strieder, Phys. Rev. C **72**, 062801 (2005).
[6] H. W. Becker, private communication.
[7] J. G. Learned, "Detection of Geo-neutrinos", presented at Neutrino 2008.
[8] B. Aharmim *et al.* [SNO], Phys. Rev. C **72**, 055502 (2005).
[9] J. N. Bahcall *et al.*, Astrophys. J. **621**, L85 (2005).
[10] JAIF, the Japan Atomic Industrial Forum. http://www.jaif.or.jp/english/